ICESat-2 melt depth retrievals: application to surface melt on Amery Ice Shelf, East Antarctica

Helen Amanda Fricker[1], Philipp Arndt[1], Kelly M. Brunt[2,3], Rajashree Tri Datta[2,3], Zachary Fair[4], Michael F. Jasinski[2], Jonathan Kingslake[5], Lori A. Magruder[6], Mahsa Moussavi[7,8], Allen Pope[7,8], Julian J. Spergel[4], Jeremy D. Stoll[2], Bert Wouters[9,10]

[1]Institute of Geophysics and Planetary Physics, Scripps Institution of Oceanography, University of California, San Diego, La Jolla, CA, USA

[2]NASA Goddard Space Flight Center, Greenbelt, MD, USA

[3]Earth System Science Interdisciplinary Center, University of Maryland, College Park, MD, USA

[4]University of Michigan, Ann Arbor, MI, United States

[5]Department of Earth and Environmental Sciences, Lamont-Doherty Earth Observatory of Columbia University, Palisades, NY

[6]Applied Research Laboratories, The University of Texas at Austin, Austin, TX and Department of Aerospace Engineering and Engineering Mechanics, The University of Texas at Austin, Austin, TX.

[7]National Snow and Ice Data Center, Boulder, CO USA

[8]Cooperative Institute for Research in Environmental Sciences, University of Colorado, Boulder, CO USA

[9]Institute for Marine and Atmospheric research Utrecht (IMAU), University of Utrecht, NL

[10]Department of Geoscience & Remote Sensing, Delft University of Technology, NL

Corresponding author: Helen Amanda Fricker (hafricker@ucsd.edu)

Key Points:

- ICESat-2 photons penetrate surface melt lakes and reflect from both the water surface and the underlying ice, providing depth estimates.
- We compared depths from eight algorithms (six ICESat-2 and two image-based) for four lakes present on Amery Ice Shelf in January 2019.
- Depths from ICESat-2 were more accurate than from imagery (30-70% too low); merging these data will improve estimates ice-sheet wide.

This is the author manuscript accepted for publication and has undergone full peer review but has not been through the copyediting, typesetting, pagination and proofreading process, which may lead to differences between this version and the Version of Record. Please cite this article as doi: 10.1029/2020GL090550.

Abstract

Surface melting occurs during summer on the Antarctic and Greenland ice sheets, but the volume of meltwater stored has been difficult to quantify due to a lack of accurate depth estimates. NASA's ICESat-2 laser altimeter brings a new capability: photons penetrate water and are reflected from both the water and the underlying ice; the difference provides a depth estimate. ICESat-2 sampled Amery Ice Shelf on 2 January 2019 and showed double returns from surface depressions, indicating meltwater. For four melt features, we compared depth estimates from eight algorithms: six based on ICESat-2 and two from coincident Landsat-8 and Sentinel-2 imagery. All algorithms successfully identified surface water at the same locations. Algorithms based on ICESat-2 produced the most accurate depths; the image-based algorithms underestimated depths (by 30-70%). This implies that ICESat-2 depths can be used to tune image-based algorithms, moving us closer to quantifying stored meltwater volumes across Antarctica and Greenland.

Plain Language Summary

Summer surface melting on Antarctica's ice shelves is a small component of overall ice sheet mass loss but can be important for individual ice shelves and may increase as climate warms. However, the volume of meltwater has been difficult to monitor because depth estimates are challenging. NASA's ICESat-2 laser altimetry mission brings a new capability to this problem. ICESat-2 532 nm photons (green light) are able to pass through water and reflect from both the water surface and the underlying ice surface; the difference in elevation provides meltwater depth estimates. In this pilot study we compared depths from eight algorithms (six ICESat-2 and two image-based) over four Amery Ice Shelf meltwater lakes for an ICESat-2 pass in early January 2019. The ICESat-2 algorithms all produced more reliable depth estimates, and the image-based algorithms underestimated the depths. This implies that ICESat-2 water depths can be used to tune image-based depth retrieval algorithms, enabling improved performance and allowing us to estimate more accurately how much surface melt is stored in melt ponds on the ice sheets each summer.

1. Introduction

Antarctica's ice shelves are losing net mass to the ocean, mainly through iceberg calving and basal melting (*Adusumilli et al.*, 2020; *Rignot et al.*, 2013). While surface melt does not yet significantly impact overall mass balance, it is widespread on Antarctica's ice shelves (e.g., *Zwally and Fiegles*, 1994; *Trusel et al.*, 2012) and is predicted to increase (*Trusel et al.*, 2015). Over the last decade, widespread and rapid changes have been observed in some regions of the Antarctic Ice Sheet, including thinning (*Shepherd et al.*, 2003, *Fricker and Padman*, 2012; *Paolo et al.*, 2015) and dramatic disintegration of Antarctic Peninsula ice shelves through hydrofracture (*Rott et al.*, 1996; *Scambos et al.*, 2003). Although no major changes on this scale have been identified in the East Antarctic Ice Sheet (EAIS; which contains approximately 75% of the total Antarctic ice sheet area, 85% of the volume, and accounts for 52 m of potential sea-level rise (*Lythe et al.*, 2000)), there is a possibility that areas of the EAIS could become more vulnerable to hydrofracture as atmospheric temperatures increase and surface melt increases (*Kingslake et al.*, 2017; *Bell et al.*, 2018; *Lai et al.*, 2020). Therefore, it is important to monitor amount of meltwater current produced each year. Supraglacial lakes are one important destination for surface meltwater; others include firn (via refreezing and storage in aquifers), and the ocean (through dolines and off the front of ice shelves). Therefore, one way to monitor the state of the ice sheet's supraglacial hydrology is to quantify the amount of water stored in lakes, but this has been challenging, due to lack of accurate depth estimates. Therefore, there are no comprehensive estimates of total meltwater produced each melt season.

Amery Ice Shelf experiences annual surface melt, and previous studies indicate interannual variability in meltwater timing and duration and the extent of the drainage system (*Phillips*, 1998; *Spergel et al.*, 2020). In this paper, we introduce a new technique for estimating melt water depth from ICESat-2 data and demonstrate it on Amery Ice Shelf, EAIS, during the January 2019 melt season. We describe a pilot project with investigators who contributed depth estimates for four Amery melt lakes along a single ICESat-2 ground track. We used eight algorithms to estimate the depth of meltwater stored in melt features: six based on ICESat-2 data (five semi or fully automated algorithms in various stages of development, and one manual method, used as a baseline for comparison in the absence of ground truth); and two based on imagery (Sentinel-2 and Landsat 8). We compared the results from the ICESat-2 algorithms and then compared the ICESat-2 depth estimates with depth estimates from Landsat 8 and Sentinel-2 satellite imagery. Although ICESat-2 provides water depth estimates solely along its ground tracks and has limited spatial sampling of short-lived melt features, the ICESat-2 derived depth estimates can provide a training dataset for image-based methods, which can then be extended to provide depth estimates across entire melt regions. This will significantly improve our capability to estimate the volume of surface melt stored in surface lakes on each ice sheet.

2. Previous observations of Amery surface melt

Amery Ice Shelf (area 70,000 km^2) is EAIS's largest ice shelf, and buttresses the largest drainage basin in EAIS (Lambert-Amery system); this basin drains ~16% of the area and ~14% of the volume of the EAIS, with 7.7 m of sea-level potential (*Tinto et al.*, 2019). Located between 69°S and 73°S, Amery Ice Shelf is far enough north that it experiences significant surface melting each summer (*Phillips*, 1998; *Kingslake et al.*, 2017), and it has been suggested that it may be susceptible to breakup within a few decades if it experiences warming trends similar to those which took place on the Peninsula (*Scambos et al*., 2003). The onset date, freeze over date and duration of surface melting vary from year to year; these are all climate-related variables that can be monitored with satellite remote sensing (*Phillips*, 1998; *Tedesco*, 2007; *van den Broeke*, 2005).

Surface melt features on southern Amery Ice Shelf were documented as early as 1960, when it was noted that extensive summer melting took place forming rivers, melt lakes and dolines (*Mellor and Mackinnon,* 1960). They have also been detected by aerial observation, in synthetic aperture radar (SAR) and Landsat satellite imagery and in satellite radar altimetry (e.g. *Swithinbank et al.*, 1988; *Phillips*, 1998). Surface melting occurs in the blue-ice zone near the grounding line. Meltwater mostly collects in longitudinal-to-flow topographic depressions between glacier flowlines, which transport water downstream towards the center of the ice shelf as "meltstreams" (Figure 1). Surface melt features are spatially extensive, and individual meltstreams and lakes can be several km wide. These meltwater systems are active in most summers, carrying large volumes of meltwater and exhibiting considerable interannual variability (*Spergel et al.,* 2020).

A previous Amery study (*Phillips*, 1998) showed that meltwater in the surface depressions changes the shape of ERS-1 radar altimetry waveforms: one meltstream was sufficiently wide (~2 km) to create a bright target on the surface, leading to a specular return. Specular returns were detected in 3-day repeat data in the 1992/93 and 1994/95 melt season; the short repeat time allowed for a precise constraint on onset time and duration. This provided limited information about interannual variability of melt onset, extent and duration. However, this was only for two melt seasons, and there was no estimate of meltwater depth, so it did not allow for monitoring the surface volume.

ICESat-2 data over Amery meltwater lakes

ICESat-2 carries the Advanced Topographic Laser Altimeter System (ATLAS), which is a photon-counting, 532 nm (green light) lidar operating at 10 kHz. ATLAS splits the transmitted laser pulse into six beams, to form three pairs (each pair containing one weak and one strong beam, separated by 90 m) 3.3 km apart. Each beam has a ground-footprint of ~17 m in diameter (estimated to be closer to ~11 m from on-orbit assessments; *Magruder et al.*, in review), offset by 0.7 m along-track. This beam configuration and acquisition design provides a snapshot of surface slope along each ground track, while also obtaining six times more observations than a single beam. ICESat-2's 1387 unique reference ground tracks (RGTs) extend to 88°, and it samples them four times a year (91-day repeat cycle) in the polar regions. ICESat-2 began pointing to the planned RGTs in late March 2019 once the on-orbit pointing calibrations were determined and updated within the on-board pointing control systems (*Martino et al.*, 2019); thus, the early ICESat-2 observations used here were not repeat tracks within the current 91-day cycle. Over ice sheets, ICESat-2 has demonstrated better than 13 cm of surface measurement precision (1-sigma standard deviation), based on assessments of both the ATL03 and ATL06 data products (*Brunt et al.*, 2019).

We identified an ICESat-2 pass over the southern Amery Ice Shelf during the 2018/2019 melt season, that had contemporaneous Landsat-8 and Sentinel-2 imagery: Track 0081 on 2 January 2019. We examined both Level-2 (ATL03; *Neumann et al.*, 2019) and Level-3a (ATL06 Land Ice Product; *Smith et al.*, 2019a) ICESat-2 products. ATL03 data contain the full stream of returned photons (*Neumann et al.*, 2019), geolocated and classified as high, low or medium confidence of representing the surface. ATL03 data showed double returns located in surface depressions, indicating meltwater (Figure 2). ATL06 data contain averaged elevations for one surface only, based on ATL03 data for 40 m overlapping segments at 20 m spacing, is optimized for ice surfaces, and was developed in the years leading up to launch. ATL06 heights cannot be used to examine meltwater features that create a second surface (Figure 1); this application requires analysis of the ATL03 photon data, which requires new algorithms.

ICESat-2 water depth estimates

ICESat-2 approaches to estimating lake depths require separation of the water surface and underlying ice topography from the ATL03 photon cloud. We tested six algorithms for this application that have been developed less than two years since launch and are in various stages of development (Table 1):

(i) Adapted ATL08 algorithm: this approach is derived from an existing algorithm developed for the ATL08 land and vegetation along-track product (*Neuenschwander & Pitts*, 2019). ATL08 leverages both the ATL03 signal finding approach and an alternative method for noise filtering. The algorithm work flow is unique amongst the ICESat-2 along-track geophysical products with its ability to segregate the return signal into multiple surfaces. In the traditional ATL08 implementation, these segregated surfaces represent canopy heights and terrain heights respectively, using statistical signal classification for each type. For application over melt ponds, we implemented the ATL08 signal finding and surface classification schemes based on ATL03 input similar to the traditional approach, but applied them in reverse order: the ground-finding component to the water surface and the top of canopy height extraction to the melt lake bottom. That is, we reconfigured the ATL08 algorithm to perform top-down analysis for segregation of water and underlying ice rather than the bottom-up approach used for land and vegetation. Looking forward, since ATL08 identified points are indexed to ATL03, the fundamental ATL08 algorithm components (signal finding, point classification and multi-surface interpretation) can be further optimized to exploit the observed bathymetric signatures associated with the water column and radiometry of the water/lake bottom ratios at range of along-track resolutions.

(ii) ATL13-melt.v1: this method estimates along track depths at discrete points using a modified version of the operational depth algorithm developed for the ATL13 Inland Water Data Product (*Jasinski et al.*, 2019). We assume that meltwater pond boundaries are approximately known, and exact boundaries are refined by anomaly analysis. Surface mean height and standard deviation are computed using a quasi-physical statistical model. Surface signal photons are analyzed for along-track, 50-signal photon short segments, aggregated to longer segments as necessary. Depth profile retrievals include deconvolution of the ATLAS Impulse Response Function from the observed profile. Bottom analysis begins several surface height standard deviations (default 12 sigma) or 6 m below the mean surface, whichever is deeper. Histograms of the long segment vertical profiles are evaluated at three elevation levels of confidence with the highest confidence attributed to bottom. Depth is computed as the difference between the mean surface and mean bottom elevations.

(iii) Lake surface-bed separation (LSBS; *Fair et al.*, 2020): this method uses ATL03 data to separate lake features into distinct arrays for the surface and bed. LSBS is accomplished by distributing ATL03 data into elevation bins, with the expectation that water surfaces are easily identifiable in histograms of high confidence photons. Once a lake surface is identified, statistical inference is used to derive an initial guess for the lake bed topography. To improve the estimation, we also incorporate photon refinement procedures developed for the ATL06 surface finding algorithm (*Smith et al.*, 2019). With this approach, the window for acceptable signal photons is a function of the residuals of photons relative to the regression. The accepted photons then provide a "best guess" for the surface and bed of melt lakes, from which water depth is calculated. (To compare with *Fair et al.*, 2020, our Lakes 1, 3 and 4 are their Figures 4a, 4b and 4d respectively).

(iv) Watta (*Datta & Wouters*, submitted): uses ATL03 data to identify the surface and bottom of a lake as well as potential intermittent ice layers. This method identifies the first three maxima of an adaptive kernel density estimate of elevation values for photons over a moving along-track footprint and then assigns types for (i) surface (ii) ice on surface (ii) subsurface ice (iv) bottom based on the relative height and strength of the signal. The algorithm has been tested with ATLAS's strong and weak beams with a mix of photon confidence levels. It was developed and evaluated over Western Greenland during the 2019 melt season, with lakes at all times throughout the season. For 14 of these cases, we were able to collect same-day high-resolution imagery from Planet SkySat, which we used both to validate the surface as well as to extract total melt volumes.

(v) Surface Removal and Robust Fit (SuRRF): This method requires as input a segment of ATL03 data that is known to contain a *single* melt lake. It finds the flat water surface in ATL03 data by histogram-binning the entire segment and finding the peak, then removes all photons corresponding to that surface. Then, a smooth line is fit to the remaining photon data (all ATL03 photon confidences), using a robust, locally weighted moving average. For all locations where the elevation of the final smooth line is lower than the elevation of the lake surface, the water depth is the difference between the two. At all other locations, water depth is set to zero. See Text S1 for a complete description of this algorithm.

(vi) Manual picking: this is a manual approach used to generate a manual baseline, as a guide for true water depth in the absence of *in situ* ground truth data. We created an interactive tool in which users can draw their own best-guess estimate of the melt lake surface and bottom elevations on ATL03 photon data plots. For each contribution, both elevations were interpolated to a fine common grid and depth was calculated as the difference. We received a total of 56 depth estimates, twelve of which came from researchers on the ICESat-2 Science Team or members of their groups who work with ATL03 data (see Acknowledgements). The differences in depth between the mean of these 12 “expert estimates” and the mean of the remaining estimates were insignificant, with a bias of 2.2 cm and a standard deviation of 6.6 cm. Therefore, we used all 56 manual estimates to construct a “baseline” ensemble estimate, to compare with all other algorithms. To make this ensemble robust to outliers, we used the mean of all depth estimates falling within the middle quartiles at each location.

Image-based water depth estimates

We used a light attenuation algorithm physically-based model widely used for supraglacial lake depth retrieval in Greenland and Antarctica (e.g., *Sneed & Hamilton*, 2011; *Tedesco & Steiner*, 2011). We applied the following expression to Landsat-8 and Sentinel-2 multi-spectral imagery:

$$z = [\ln(A_d - R_\infty) - \ln(R_w - R_\infty)] / g,$$

where A_d is the albedo of the lake bed, R_∞ is the reflectance of optically deep water (>40 m), R_w is the observed water reflectance, z is water depth, and g is a two-way attenuation coefficient. The values of A_d, R_∞ and g depend on the imagery and band used. We identified lake pixels by thresholding the Normalized Difference Water Index (NDWI) (*Moussavi et al.*, 2020), and estimated A_d by averaging reflectances over a three-pixel-wide ring around each lake and R_∞ as the 5th percentile Top Of Atmosphere (TOA) reflectance in nearby coastal tiles that included ocean pixels. In Landsat-8 images, we used *g* derived from depth measurements from Greenland and Antarctic lakes (*Pope et al.*, 2016; *Pope*, 2016; *Moussavi et al.*, 2020), and averaged the depths from the red band and the panchromatic band to produce the final depth estimate. We used Landsat-8 images from 2 January 2019. In Sentinel-2 images (also 2 January 2019), we estimated depths from the red band, using g=0.83 (*Williamson et al.*, 2018).

Comparison of water depth estimates

We used ATL03 Release 003 data (*Neumann et al.*, 2020) for the central strong beam (GT2L) of a single repeat of ICESat-2 Track 81 across Amery Ice Shelf, 2 Jan 2019. The acquisition time was near the peak of the melt season, and was the same day as available Landsat-8 and Sentinel-2 images. The track sampled several locations with substantial surface water bodies and we selected four of these, as highlighted in *Magruder et al.* (2019) (Figure 1). These four melt lakes represent a variety of widths (~800 m to 2 km) and depths (~1 m to 6 m).

For some of the melt lakes there is an “after event”, which manifests as an apparent second flat return surface located between 0.5 and 4.2 m below the water surface (e.g. Figure 1, Lake 2). These are the result of the ATLAS transmit pulse shape and the instrument response when the detectors are temporarily saturated by strong surface returns. For the purposes of this analysis we ignored these subsurface returns.

We ran all of the ICESat-2 depth retrieval algorithms over this 150 km section of track. We also ran depth estimates for the two Landsat-8 and Sentinel-2 images that were acquired across the region sampled by the track on the same day, and interpolated the image-based results to the ground track locations for comparison with the ICESat-2 depth retrievals.

Since the image-based depth estimates are of true water depth, we multiplied them by the refractive index for freshwater at 532 nm (1.33; *Parrish et al.*, 2019) so that they could be qualitatively compared against the “manual baseline” (Figure 2). For quantitative comparison of absolute depth values, however, we performed this correction in the opposite way: i.e., we corrected the ICESat-2 depths for refractive index.

Results and Discussion: differences between water depth estimates

Accuracy of manual baseline data: The manual picking method tends to place the lake bed at the elevations below the flat water surface at which photon density first increases significantly again (Figure 2), while the ICESat-2-based algorithms tend to place it closer to the second peak in photon density (*i.e.* deeper). Over land-ice surfaces, the ATL06 algorithm uses the latter approach, and has been validated to be accurate to better than 3 cm with better than 9 cm of surface measurement precision (*Brunt et al.*, 2019). However, while traveling through water, many photons in the ICESat-2 laser beams are subject to multiple scattering, which biases those photons' registered elevations towards lower elevations. While the effect of multiple scattering suggests that the true lake bed may be shallower than the elevation of peak photon density, depth is likely underestimated when using the first (shallowest) increase in photon density. This is because in the presence of an across-track slope, a first increase in density would always be due to the photons returned from the highest point within ICESat-2's ~11 m footprint. Furthermore, there will always be a spread of photons about a surface based on the pulse width of the beam; typically, we see a spread of about 25 cm. Therefore, we believe that the true depths of the melt lakes are actually a few centimeters deeper than the manual baseline estimates. In addition to this potential depth bias, the manual method is an ensemble of 56 individual estimates and thus tends to smooth out not only noise and artifacts, but also some structural details in the photon data. However, in the absence of ground truth data for the lakes considered in this study, we used the manual picking data as a proxy for the true depths (a "manual baseline"). Using the manual baseline for comparison, we assessed the performance (qualitatively and quantitatively) of each meltwater depth retrieval algorithm.

Qualitative comparison with manual baseline: In general, all algorithms (ICESat-2 and image-based) primarily identified supraglacial water at the same locations, and the along-track widths they estimated were approximately the same for each meltwater feature, and consistent with the manual baseline. Broadly speaking, the shape of all lakes (how the depth changes with distance along track) are qualitatively similar, and depth maxima were in approximately the same locations on the track; however the absolute depths were different for all algorithms (Figure 2). All ICESat-2 algorithms captured different amounts of structural detail. Overall, the techniques that use the ICESat-2 data produced depths closest to the manual baseline, with the closest estimate being the ATL08 technique. This is because the ATL08 algorithm estimates the surface from the median value, which places its derived surface below the "top" of the lake bottom returns, similar to the manual baseline. LSBS produced false positives between the lobes of lakes 3 and 4, i.e. estimated depths over non-melt areas; LSBS had no depth estimate for the northern lobe of lake 2.

Quantitative comparison with manual baseline: Overall, the five algorithms based on ICESat-2 produced depths that were much closer to the manual baseline than the image-based algorithms. Most ICESat-2 based algorithms show a bias towards deeper depths when compared to the manual baseline (Figure S1). The ATL08 algorithm produced the estimates that were closest to the manual baseline (mean of differences is 0.02 m, standard deviation 0.2 m). We averaged the depth estimates from the five ICESat-2 algorithms to form an ICESat-2 "ensemble"; the ensemble mean lies mostly at deeper depths, and the mean of the differences between the ICESat-2-based estimates and the manual baseline is -0.13 m (the ICESat-2 depths are deeper than the manual baseline). However, the standard deviation of differences between the depths from the manual baseline and the ICESat-2 algorithm ensemble (0.17 m) is lower than that of any single algorithm, so the ensemble lake bottom fits the general "shape" of the lake bottom better; implying that the ultimate meltwater retrieval algorithm will combine aspects of all five algorithms.

For these four lakes, both image-based techniques produced meltwater depth estimates that were too shallow: the mean of the differences between the image-based estimates and the manual baseline is +0.71 m (the image-based depths are shallower than the manual baseline); the standard deviation is 0.75 m, i.e., average depths were 70% too low for the Landsat-8 technique and 30% for Sentinel-2. This large difference between Landsat-8 and Sentinel-2 estimates for these four lakes is not consistent with (*Moussavi et al.)* 2020 based on a larger sample of 42 Landsat-8 – Sentinel-2 imagery pairs. They showed that, while the depths of individual lakes measured with Sentinel-2 and Landsat-8 varied, overall there was reasonable agreement between the two approaches. However, the fact that ICESat-2 depths are more accurate for the same lakes implies that ICESat-2 depths can be used to tune image-based algorithms.

ICESat-2 algorithm automation and efficiency: Since ICESat-2 operates continuously and has six beams, there is a potential for a vast amount of ICESat-2 data for any given melt season. It is not efficient to search through all the ATL03 data for melt features, even when surface water persists only for weeks to months each year on each ice sheet. This means that an automated algorithm will ultimately be required. The ICESat-2 algorithms we considered are in various stages of development and have varying levels of automation; most of them are only partially automated (Table 1). As we showed here, the search domain can be narrowed using contemporaneous imagery to identify potential regions of surface water. In the absence of this imagery we propose that the ATL06 data themselves could be used to locate potential regions of standing surface water (based on the fact that their surfaces are flat, which could be searched for using ATL06 slope estimates). This approach would not work, however, if the meltwater is flowing.

Summary

After only a few months on orbit, ICESat-2 acquired data during an Antarctic melt season (2018-2019). Using ICESat-2 ATL03 (full photon) data from one ground-track across Amery Ice Shelf, EAIS at the peak of the melt season (January 2019), we demonstrated that the ICESat-2 signal penetrates the surface meltwater; photons are returned from both the water surface and the underlying ice surface. ICESat-2 operates continuously and has six beams, producing large amounts of ATL03 ICESat-2 data each melt season. Therefore, it is desirable to find a technique to locate both the surface meltwater and underlying ice surface in the data, and automatically provide an accurate estimate of the distance between the two (the meltwater depth). Since this capability of ICESat-2 was realized, several algorithms have been developed to estimate water depth estimates.

We performed a pilot study where we compared depth estimates from six different ICESat-2 algorithms in various stages of development and two image-based algorithms for four melt lakes on 2 January 2019. To assess the estimates, we created a baseline using a manual picking technique based on ICESat-2 data. All algorithms were equally reliable in detecting the presence of surface melt; however, the ICESat-2 based algorithms provided most accurate melt depth estimates, with the estimates from the adapted ATL08 algorithm being the closest to the manual baseline. The image-based algorithms tended to underestimate melt depths by 30-70%. While this study presents results for just four lakes on one ice shelf, since the Landsat-8 has been used for most meltwater depth estimates around Antarctica and Greenland to date, it is likely these estimates are too low. ICESat-2 melt depths will allow us to improve the performance of image-based approaches that have better spatial coverage, or even to examine the performance of supervised statistical learning algorithms trained on ICESat-2 depths, moving us closer to an assessment of total meltwater produced each melt season across Antarctica and Greenland.

Figures

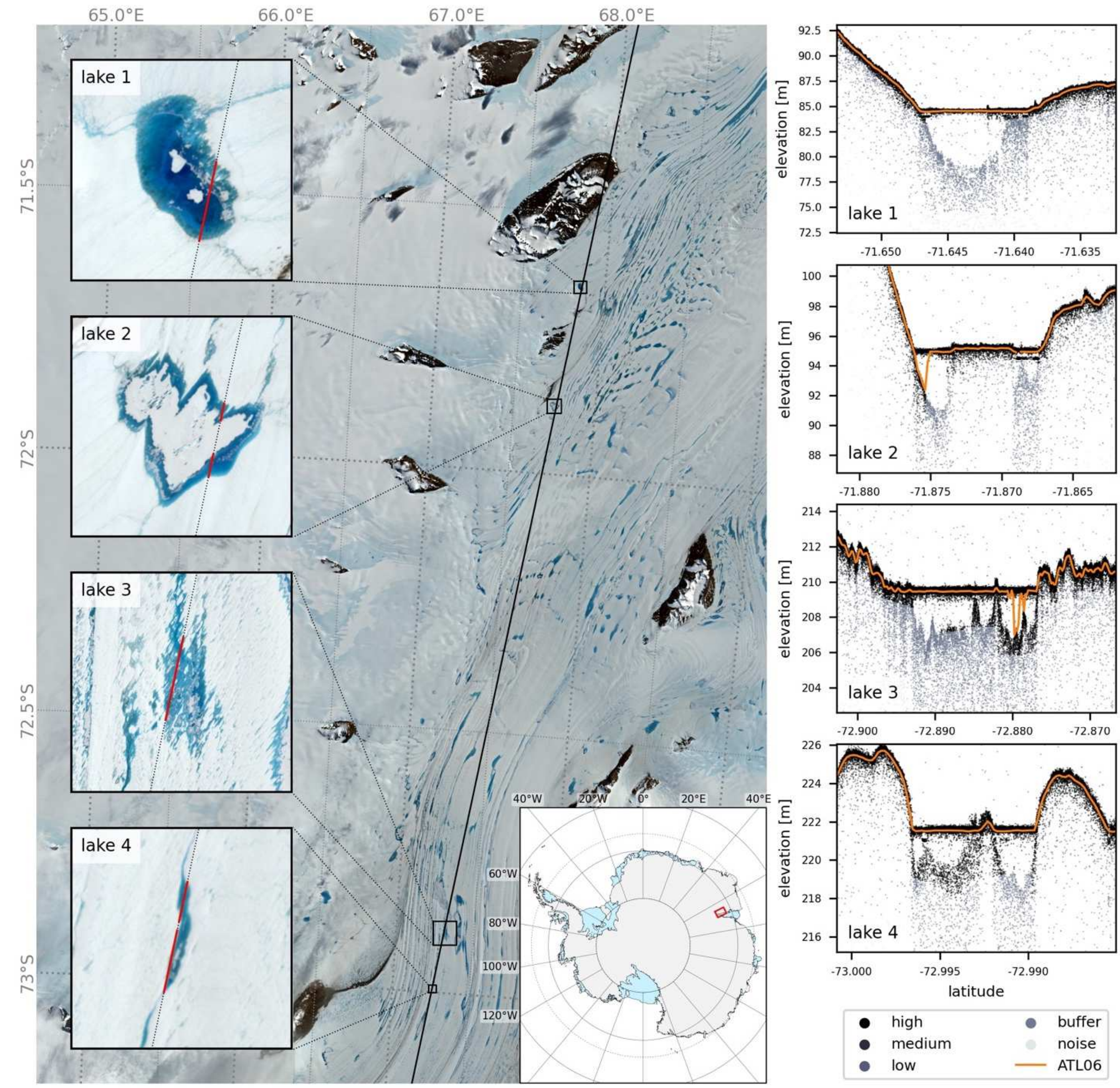

***Figure 1**:* Left: Sentinel-2 image over Amery Ice Shelf, 2 January 2019 showing ICESat-2 ground track 0081 GT2L acquired on the same day. The magnified areas show the four melt lakes considered in this study. Right: ATL03 data for the four melt lakes, with each photon colored by its confidence level for being a land-ice surface signal. ATL06 surface elevations are also shown.

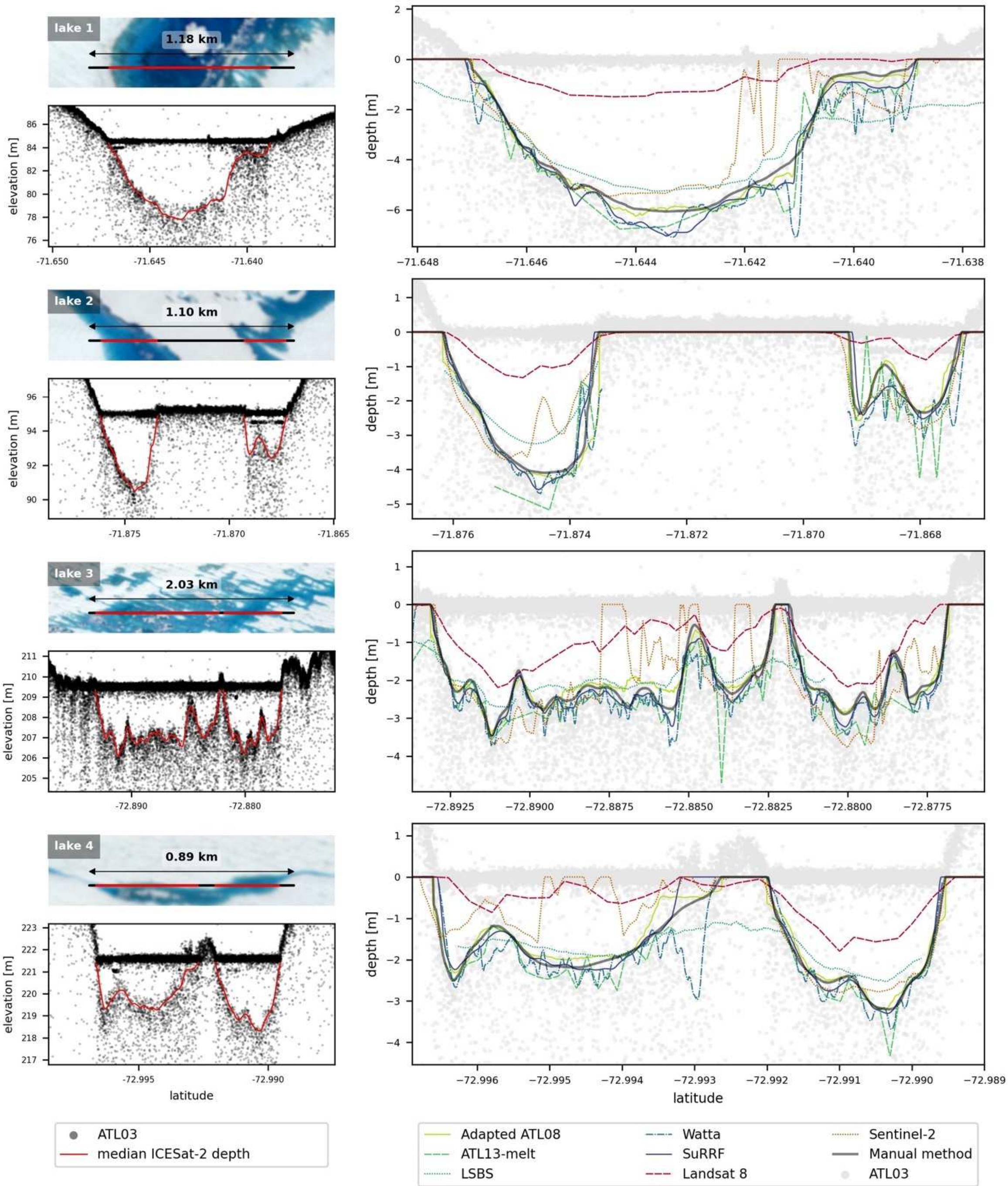

Figure 2. Left panels: ICESat-2 ATL03 photon data over the four melt lakes used in this study, with median depth estimates from the ICESat-2 algorithms shown in red. Above each plot are the corresponding same day Sentinel-2 images, showing the location of the ICESat-2 ground track segment. Right panels: Comparison of depth estimate retrievals for each lake. To aid visual comparison, image-based estimates have been multiplied by refractive index, and background topography has been removed.

Table 1. Main characteristics of the six ICESat-2 melt depth algorithms used in this study: level of automation, research goal, and known advantages and disadvantages.

Algorithm	Level of Automation	Research goal	Advantages	Disadvantages
i) Adapted ATL08	Fully automated extraction of water surface and sea floor in ATL03 transect for coastal regions. Semi-automated for melt ponds.	Shallow water coastal bathymetry for benthic habitat mapping	Photon level resolution. Classifies signal as surface, sea floor or water column for further aggregation or analysis	Limited to ATL03 input and hasn't been adapted to accommodate signal artifacts due to detector saturation
ii) ATL13-melt.v1	Automated with *a priori* knowledge of a melt lake being present within an ATL03 segment	Inland and near shore hydrology for melt lakes, ponds and streams	Continuous, along track open water surface height statistics and slope; Along track depth at discrete points, 15-50m spatial resolution	Results limited to only along track profiles for each beam.
iii) LSBS	Automated with *a priori* knowledge of a melt lake being present within an ATL03 segment	Supraglacial lake depth retrievals	Distinguishes between lake surface and bed. Retrieves depths for deep lakes. Performs retrievals for ICESat-2 and ATM	Detection of small lakes (< 200 m in diameter) is difficult with ICESat-2. Uncertainties may increase when noise at the lake bed is significant
iv) Watta	Fully automated	To detect melt lake depth, ice over a lake, ice under the surface of a lake, slush, refrozen melt lakes. Feature types assigned probabilistically, accounting for signal saturation	Can be used under multiple beam/cloud conditions with associated quality flags. Detects small-scale bathymetry	Detection of slush and water flowing downstream still in development. More sensitive to outliers due to minimal smoothing (to capture smaller-scale features)
v) SuRRF	Automated with *a priori* knowledge of a *single* melt lake being present within an ATL03 segment	Supraglacial lake depth retrievals, to use in combination with satellite imagery	Robust even with high levels of background noise, smoothly tracks the ice surface at lake edges	Does not work if the water surface is not flat (i.e. flowing water with an along-track surface gradient), tends to smooth out fine-scale details
vi) Manual method	No automation	Provides an approximate baseline for comparison with image-based and ICESat-2 based retrievals	Captures the approximate depth and shape of melt lakes without large outliers.	Depth estimate is a subjective visual best guess of where the surface/bed and may be biased; fine-scale details are smoothed out by taking an ensemble

Acknowledgments, Samples, and Data

We would like to thank the 56 people (ICESat-2 researchers, UCSD students, and family/friends) who contributed manual depth estimates using the Python script at https://github.com/fliphilipp/pondpicking. We would like to thank our colleagues (on the ICESat-2 Science Team and the broader community) for useful discussions about this paper, especially Susheel Adusumilli, Maya Becker, Ute Herzfeld, Alex Gardner, Laurie Padman, Ben Smith and Roland Warner. All data and code needed to produce the figures in this manuscript are available on Zenodo: https://doi.org/10.5281/zenodo.4299237. We received funding from various sources, as follows: NASA NNX15AC80G (Fricker and Arndt); NASA ICESat-2 Project Science Office (Brunt and Datta); NASA 19-EARTH19R-0047 (Fair and Flanner); NASA (Jasinski and Stoll); NSF-OPP 1743310 (Kingslake and Spergel); NASA NNX15AC68G (Magruder); NSF Grant 1643715 (Moussavi and Pope); NWO VIDO grant 016.Vidi.171.063 (Wouters).

References

Adusumilli, S., H. A. Fricker, B. Medley, L. Padman, & M. R. Siegfried (2020) Interannual variations in meltwater input to the Southern Ocean from Antarctic ice shelves, *Nature Geoscience*, https://doi.org/10.1038/s41561-020-0616-z.

Bell, R.E., Banwell, A.F., Trusel, L.D. & J. Kingslake (2018) Antarctic surface hydrology and impacts on ice-sheet mass balance. *Nature Climate Change*, 8**,** 1044–1052 (2018). https://doi.org/10.1038/s41558-018-0326-3.

Brunt, K.M., T.A. Neumann, & B.E. Smith (2019). Assessment of ICESat-2 ice-sheet surface heights, based on comparisons over the interior of the Antarctic ice sheet. *Geophysical Research Letters*, 46(22), 13,072-13,078, doi:10.1029/2019GL084886.

Cook, A. J. & D. G. Vaughan (2010). Overview of areal changes of the ice shelves on the Antarctic Peninsula over the past 50 years. *The Cryosphere*, 4(1):77–98.

Datta, R. and B Wouters, Supraglacial lake bathymetry automatically derived from ICESat-2 constraining lake depth estimates from multi-source satellite imagery, submitted to *Geophysical Research Letters*.

Fair, Z., M. Flanner, K. M. Brunt, H. A. Fricker, & A. S. Gardner (2020) Using ICESat-2 and Operation IceBridge altimetry for supraglacial lake depth retrievals, *The Cryosphere Discussions*, https://doi.org/10.5194/tc-2020-136.

Fricker, H. A., & L. Padman (2012). Thirty years of elevation change on Antarctic Peninsula ice shelves from multimission satellite radar altimetry. *Journal of Geophysical Research: Oceans*, *117*(C2).

Jasinski, M., J. Stoll, D. Hancock, J. Robbins, J. Nattala, T. Pavelsky, J. Morrison, B. Jones, M. Ondrusek, C. Parrish & the ICESat-2 Science Team (2019) Algorithm Theoretical Basis Document (ATBD) for Inland Water Data Products, ATL13, Version 2, Release Date October 1, 2019, NASA Goddard Space Flight Center, Greenbelt, MD, 99 pp. https://doi.org/10.5067/3H94RJ271O0C.

Kingslake, J., Ely, J. C., Das, I., & Bell, R. E. (2017). Widespread movement of meltwater onto and across Antarctic ice shelves. *Nature*, 544 (7650), 349-352.

Lai, C., Kingslake, J., Wearing, M.G., P-H. C. Chen, P. Gentine, H. Li, J. J. Spergel & J. M. van Wessem (2020) Vulnerability of Antarctica's ice shelves to meltwater-driven fracture. *Nature* 584, 574–578 (2020). https://doi.org/10.1038/s41586-020-2627-8.

Lythe, M. B., & Vaughan, D. G. (2001). BEDMAP: A new ice thickness and subglacial topographic model of Antarctica. *Journal of Geophysical Research: Solid Earth*, *106*(B6), 11335-11351.

Magruder, L., K. M. Brunt, T. Neumann, B. Klotz, & M. Alonzo (in review) Passive ground-based optical techniques for monitoring the on-orbit ICESat-2 1 altimeter geolocation and footprint diameter. *Earth and Space Science*. See attached PDF.

Martino, A. J., Neumann, T. A., Kurtz, N. T., & McLennan, D. (2019). ICESat-2 mission overview and early performance. In *Sensors, Systems, and Next-Generation Satellites XXIII* (Vol. 11151, p. 111510C). International Society for Optics and Photonics.

Moussavi, M., A. Pope, A. R. W. Halberstadt, L. D. Trusel, L. Cioffi, & W. Abdalati (2020). Antarctic Supraglacial Lake Detection Using Landsat 8 and Sentinel-2 Imagery: Towards Continental Generation of Lake Volumes. *Remote Sensing*, *12*(1), 134.

Neuenschwander, A.L., & K. Pitts (2019). The ATL08 land and vegetation product for the ICESat-2 mission. *Remote Sensing of the Environment, 221:247-259.* https://doi.org/10.1016/j.rse.2018.11.005

Neumann, T. A., A. J. Martino, T. Markus, S. Bae, M. R. Bock, A. C. Brenner, K. M. Brunt, J. Cavanaugh, S. T.Fernandes, D. W.Hancock, K. Harbeck, J. Lee, N. T.Kurtz, P. J.Luers, S. B.Luthcke, L. Magruder, T. A. Pennington, L. Ramos-Izquierdo, T. Rebold, J. Skoog, T. C.Thomas (2019) The Ice, Cloud, and Land Elevation Satellite–2 mission: A global geolocated photon product derived from the Advanced Topographic Laser Altimeter System. *Remote Sensing of Environment* 233 (2019): 111325.

Neumann, T. A., A. Brenner, D. Hancock, J. Robbins, J. Saba, K. Harbeck, A. Gibbons, J. Lee, S. B. Luthcke, & T. Rebold (2020) ATLAS/ICESat-2 L2A Global Geolocated Photon Data, Version 3. Granule: ATL03_20190102184312_00810210_003_01.h5. Boulder, Colorado USA. NASA National Snow and Ice Data Center Distributed Active Archive Center. doi: https://doi.org/10.5067/ATLAS/ATL03.003.

Paolo, F. S., H.A. Fricker, & L. Padman (2015). Volume loss from Antarctic ice shelves is accelerating. *Science*, *348*(6232), 327-331.

Parrish, C., L.A. Magruder, A. Neuenschwander, N. Forfinski-Sarkozi, M. Alonzo, & M. Jasinski, (2019) Validation of ICESat-2 ATLAS bathymetry and analysis of ATLAS's bathymetric mapping performance. *Remote Sensing,* 11 (14), doi: 10.3390/rs11141634.

Phillips, H. A. (1998). Surface meltstreams on the Amery Ice Shelf, East Antarctica. *Annals of Glaciology*, *27*, 177-181.

Pope, A., T. Scambos, M. Moussavi, M. Tedesco, M. Willis, D. Shean, & S. Grigsby (2016). Estimating supraglacial lake depth in West Greenland using Landsat 8 and comparison with other multispectral methods. *The Cryosphere* 10(1): 15-27. doi:10.5194/tc-10-15-2016.

Pope, A. (2016). Reproducibly estimating and evaluating supraglacial lake depth with Landsat 8 and other multispectral sensors. *Earth and Space Science*, *3*(4), 176-188. https://doi.org/10.1002/2015EA000125

Rignot, E., Jacobs, S., Mouginot, J., & Scheuchl, B. (2013). Ice-shelf melting around Antarctica. Science, 341(6143), 266-270.

Rott, H., Skvarca, P., & Nagler, T. (1996). Rapid collapse of northern Larsen ice shelf, Antarctica. *Science*, *271*(5250), 788-792.

Scambos, T., Hulbe, C., & Fahnestock, M. (2003). Climate-induced ice shelf disintegration in the Antarctic Peninsula. Antarctic Peninsula Climate Variability: Historical and Paleoenvironmental Perspectives, *Antarct. Res. Ser*, *79*, 79-92.

Shepherd, A., Wingham, D., Payne, T., & Skvarca, P. (2003). Larsen ice shelf has progressively thinned. *Science*, *302*(5646), 856-859.

Smith, B, H. A. Fricker, N. Holschuh, A.S. Gardner, S. Adusumilli, K.M. Brunt, B. Csatho, K. Harbeck, A. Huth, T. Neumann, J. Nilsson, & M.R. Siegfried (2019). Land ice height-retrieval algorithms for NASA's ICESat-2 photon-counting laser altimeter. *Remote Sensing of the Environment*, 233 (111352), doi:10.1016/j.rse.2019.111352.

Sneed, W. A. & Hamilton, G. S.: Validation of a method for determining the depth of glacial melt ponds using satellite imagery, Ann. Glaciol., 52, 15–22, 2011. https://doi.org/10.3189/172756411799096240

Spergel, J., J. Kingslake, T, Creyts, M. van Wessem, & H. A. Fricker (2020) Surface Meltwater Drainage and Ponding on the Amery Ice Shelf, East Antarctica, 1973-2019, submitted to *Journal of Glaciology*.

Stokes, C. R., Sanderson, J. E., Miles, B. W., Jamieson, S. S., & Leeson, A. A. (2019). Widespread distribution of supraglacial lakes around the margin of the East Antarctic Ice Sheet. *Scientific reports*, *9*(1), 1-14.

Tedesco, M. (2007). Snowmelt detection over the Greenland ice sheet from SSM/I brightness temperature daily variations. *Geophysical Research Letters*, *34*(2).

Tedesco, M & Steiner, N. (2011) In-situ multispectral and bathymetric measurements over a supraglacial lake in western Greenland using a remotely controlled watercraft, *The Cryosphere*, 5, 445–452, https://doi.org/10.5194/tc-5-445-2011.

van den Broeke, M. (2005). Strong surface melting preceded collapse of Antarctic Peninsula ice shelf. *Geophysical Research Letters*, *32*(12).

Williamson, A.G., A.F. Banwell, I.C. Willis, & N.S. Arnold (2018) Dual-satellite (Sentinel-2 and Landsat 8) remote sensing of supraglacial lakes in Greenland. *Cryosphere*, 12, 3045–3065.

Reference From the Supporting Information

Campello, R. J., Moulavi, D., & Sander, J. (2013). Density-based clustering based on hierarchical density estimates. In *Pacific-Asia conference on knowledge discovery and data mining* (pp. 160-172). Springer, Berlin, Heidelberg.